JOURNAL OF APPLIED CRYSTALLOGRAPHY

ISSN 1600-5767

Appearance of efficient luminescence energy transfer in doped orthovanadate nanocrystals

Swati Bishnoi,[a,b] G. Swati,[a,b] Paramjeet Singh,[b] V. V. Jaiswal,[b] Mukesh K. Sahu,[b] Vinay Gupta,[a,b] N. Vijayan[a,b] and D. Haranath[a,b]*

[a]Academy of Scientific and Innovative Research, CSIR – National Physical Laboratory, Dr K. S. Krishnan Road, New Delhi 110012, India, and [b]CSIR – National Physical Laboratory, Dr K. S. Krishnan Road, New Delhi 110 012, India. *Correspondence e-mail: haranath@nplindia.org

Received 31 January 2017
Accepted 16 March 2017

Edited by A. J. Allen, National Institute of Standards and Technology, Gaithersburg, USA

Keywords: phosphors; energy transfer; photoluminescence; down-conversion; nanocrystals; orthovanadate.

This paper reports the detailed synthesis mechanism and the structural, morphological and optical characterization of ultraviolet (~311 nm) excitable samarium doped gadolinium yttrium orthovanadate, (Gd,Y)VO_4:Sm^{3+}, nanocrystals. X-ray diffraction and Rietveld refinement studies confirmed that the synthesized samples crystallize in a tetragonal structure with *I*41/*amd* space group. The enhanced photoluminescence intensity of (Gd,Y)VO_4:Sm^{3+} compared with the existing YVO_4:Sm^{3+} phosphor clearly indicates the significant role of Gd^{3+} ions. This has been attributed to the sensitization of the ^6P_J energy level of Gd^{3+} ions by energy transfer from orthovanadate (VO_4^{3-}) ions and subsequent energy trapping by Sm^{3+} ions. The energy transfer from VO_4^{3-} to Sm^{3+} *via* Gd^{3+} ions as intermediates and concentration quenching of Gd^{3+} luminescence are discussed in detail. The optical band gap of the as-prepared nanocrystals has been estimated using UV–vis–NIR absorption spectroscopy, which reveals a slightly higher band gap (3.75 eV) for YVO_4 as compared to $GdYVO_4$ (3.50 eV). Furthermore, confocal microcopy, decay parameters and Commission Internationale de l'Eclairage chromatic coordinates have supplemented these studies, which established the suitability of these nanophosphors for achieving spectral conversion in silicon solar cells.

1. Introduction

Solar energy harvesting through photovoltaic (PV) technologies is one of the proficient routes to meet the rapidly growing energy demands of the world. A broad range of photovoltaic techniques for solar energy harvesting have been available for more than half a century (Hisatomi *et al.*, 2014; X. Chen *et al.*, 2012; H. M. Chen *et al.*, 2012; Pinel *et al.*, 2011; Braga *et al.*, 2008; Zou *et al.*, 2001). Nevertheless, solar energy capture *via* photovoltaic cells is still a costly issue. This cost is attributable to the low power conversion efficiencies of the existing solar cells, resulting from the spectral mismatch between the energy distribution of photons in the incident solar spectrum and the band gap of the constituent semiconductor material. Luminescent materials (phosphors) capable of converting a broad spectrum of UV radiation into photons of a particular wavelength are potential candidates for resolving the spectral mismatch issue of PV cells. Many phosphors based on oxides, silicates, vanadates, oxyfluorides *etc.* have been synthesized and studied with the aim of achieving spectral conversion in solar cells (Heng *et al.*, 2016; Zhydachevskii *et al.*, 2014; Wegh *et al.*, 1999; Wei *et al.*, 2011). Out of these available materials, orthovanadates such as YVO_4 and $GdVO_4$ have received considerable attention owing to their unique spectral properties, including narrow emission bandwidths, large Stokes

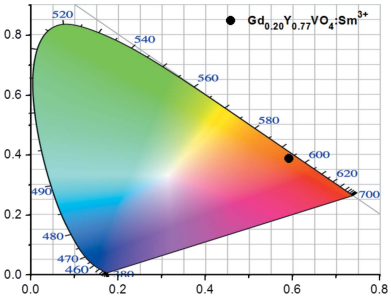

shifts, high luminescence efficiencies and longer lifetimes (Som *et al.*, 2016). Although there are many reports on $GdVO_4$ and YVO_4 based phosphors, there are very few reports on the composite $(Gd,Y)VO_4$ based nanophosphors (Som *et al.*, 2016; Kumari & Manam, 2015; Chen *et al.*, 2011; Wang *et al.*, 2009). To the best of our knowledge, this is the first report on the synthesis, mechanism, and structural and photoluminescence (PL) characterization of Sm^{3+} doped $(Gd,Y)VO_4$ based down-conversion nanophosphors. We demonstrate the role of Gd^{3+} ions as intermediates in luminescence enhancement, supported by PL and time-resolved PL decay measurements. Since the optical properties of a doped orthovanadate system depend intimately on the local structure and bonding of the dopant cations, a detailed understanding of these factors is important from a device-engineering viewpoint. The insertion of the dopant acts as a perturbation of this well studied system. Sm^{3+} was selected as a representative rare-earth ion because its unique fluorescence properties, similar to those of Eu^{3+} ions, make it an ideal probe for local structure determination of the host crystal. As a research goal to pursue, we have successfully prepared highly luminescent $(Gd,Y)VO_4:Sm^{3+}$ nanophosphor powders that have distinctive photoluminescence properties. Herein, we report a new class of highly luminescent orthovanadate based nanophosphors that individually emit orange–red luminescence on exposure to ~311 nm UV light. The advantages of the present protocol are numerous and include the following: (i) high surface-to-volume ratios with effective prevention of further aggregation of the nanophosphor particles, so as to exhibit a high luminescence yield; (ii) the profitability of size-quantized nanometre-sized $Gd_xY_{1-x}VO_4$ phosphor particles with higher redox potential, which in turn enhances the charge-transfer rates between the Gd^{3+} and VO_4^{3-} network and the dopant (Sm^{3+}) ion by host–dopant interactions; and (iii) good dispersity and useful nanodimensions for possible coating over many substrates. Furthermore, the Gd^{3+} concentration has been optimized for achieving the brightest photoluminescence. The synthesized $(Gd,Y)VO_4$ nanophosphors were characterized for their structural, morphological, optical and luminescence properties. A Rietveld refinement study of the X-ray diffraction data has been carried out to analyse the crystallographic data. The optical band gap of the samples has been approximated experimentally using UV–vis–NIR spectroscopy, which revealed a slightly higher band gap for YVO_4 as compared to $(Gd,Y)VO_4$ nanophosphors. In addition, we demonstrate that the $(Gd,Y)VO_4:Sm^{3+}$ compounds are excellent phosphors with high luminescence yields which are considered to be the best choices for achieving spectral conversion in silicon solar cells.

2. Material and methods

2.1. Synthesis of nanophosphors by co-precipitation and its detailed mechanism

$(Gd,Y)VO_4:Sm^{3+}$ nanophosphor samples were synthesized using the facile chemical co-precipitation technique. The Gd^{3+} concentration (x) was varied from 0 to 80 mol% and the Sm^{3+} concentration was fixed at 3 mol%, to achieve maximum photoluminescence emission under UV (~311 nm) excitation. For a typical sample synthesis, stoichiometric amounts of nitrate (precursor) salts of yttrium, gadolinium and samarium were dissolved in aqueous media, under continuous stirring at room temperature (~298 K). Details of the reaction mechanism are as follows.

Hydrolysis of the precursor salts gives rise to their respective hydroxides:

$$Gd(NO_3)_3 \xrightarrow{+3H_2O} Gd(OH)_3 + 3HNO_3, \quad (1)$$

$$Y(NO_3)_3 \xrightarrow{+3H_2O} Y(OH)_3 + 3HNO_3, \quad (2)$$

$$Sm(NO_3)_3 \xrightarrow{+3H_2O} Sm(OH)_3 + 3HNO_3. \quad (3)$$

Under continuous stirring at room temperature (~298 K), ammonium metavanadate (NH_4VO_3) was added dropwise. The metavanadate exists as a polymeric chain of VO_4^{3-} units:

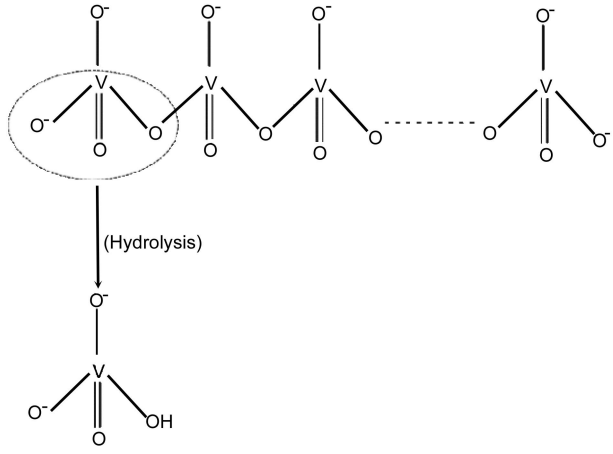

Terminal group VO_4^{3-} units undergo hydrolysis in the presence of water, which generates HVO_4^{2-} ions (acidic species). These ions do not eliminate their last H^+ ion owing to the 'common ion effect' caused by the strong acid HNO_3 existing in the solution. Subsequently, 1 *M* NaOH was added to the above solution, which reacts with HNO_3 to form a salt as a side product. The corresponding chemical reaction is

$$NaOH + HNO_3 \longrightarrow NaNO_3 \quad \text{(aqueous)}. \quad (4)$$

This salt was removed by repeated washing with demineralized water. The unreacted NaOH creates a basic medium pH > 8, which induces the reaction

$$HVO_4^{2-} + OH^- \longrightarrow \underbrace{VO_4^{3-}}_{\text{(orthovanadate ion)}} + H_2O, \quad (5)$$

$$Gd(OH)_3 + Y(OH)_3 + Sm(OH)_3 + VO_4^{3-} \longrightarrow Gd_xY_{1-x}VO_4:Sm \quad \text{(precipitate)}. \quad (6)$$

The precipitation of hydroxides occurs owing to the decrease in their solubility in the presence of traces of NaOH. In this process VO_4^{3-} replaces $3OH^-$ in the lattice stoichiometry to form the Sm^{3+} doped $(Gd,Y)VO_4$ host lattice. The resulting

precipitate was filtered off and washed several times with deionized water and ethanol, to remove the surface bound impurities and water molecules. The collected precipitate was dried in a vacuum oven and annealed at temperatures >773 K for 1–3 h.

3. Results and discussion

3.1. Crystal structure and phase analysis

For phase identification, an X-ray diffraction (XRD) analysis was carried out on Sm^{3+} doped (Gd,Y)VO_4 nanophosphors. Note that all the diffraction peaks matched very well with the standard JCPDS card (No. 85-2318; Kumari & Manam, 2015). Fig. 1(*a*) shows the XRD spectra of the as-synthesized and annealed $Gd_{0.20}Y_{0.77}VO_4$:Sm(3%) nanophosphor samples along with the standard JCPDS spectrum. Annealing at 1073 K resulted in improved crystallization as compared to the as-synthesized nanophosphor samples. The crystal structure of $Gd_{0.20}Y_{0.77}VO_4$:Sm^{3+}(3%) was confirmed and the cell parameters were calculated using Rietveld analysis as shown in Fig. 1(*b*). The phosphor crystallizes in a tetragonal structure (space group *I*41/*amd*) with the lattice constants as described in Table 1. A schematic of the structure of the $GdYVO_4$ phosphor is shown in Fig. 1(*c*).

3.2. Band gap calculations

The optical band gaps of YVO_4:Sm^{3+} and $Gd_{0.20}Y_{0.77}VO_4$:Sm^{3+} were estimated using an empirical formula known for direct band gap materials as follows:

Table 1
Cell parameters of Sm^{3+} doped $Gd_{0.20}Y_{0.77}VO_4$ nanophosphor calculated using Rietveld analysis.

Atom	*X*	*Y*	*Z*
O	0.0000	0.93874	1.46379
V	0.0000	0.96521	0.5363
Gd	0.0000	0.68983	0.42824
Y	0.0000	0.0501	−0.04051
a = 7.1624 Å	α = 90°	Cell volume = 323.9536 Å^3	R_p = 11.70
b = 7.1624 Å	β = 90°		R_{wp} = 8.10
c = 6.3148 Å	γ = 90°		R_e = 7.44
			χ^2 = 2.49

$$(\alpha h\nu)^2 = A(h\nu - E_g), \tag{7}$$

where A is a constant that depends on the transition probability, E_g is the optical band gap energy, h is Planck's constant, ν is the frequency and α is the absorption coefficient of the material. The optical band gap of the samples was calculated by extrapolating a straight line from the $(\alpha h\nu)^2$ *versus* energy (E_g) plot (Figs. 2*a* and 2*b*). The band gap values estimated for YVO_4 and (Gd,Y)VO_4 are 3.75 and 3.50 eV,

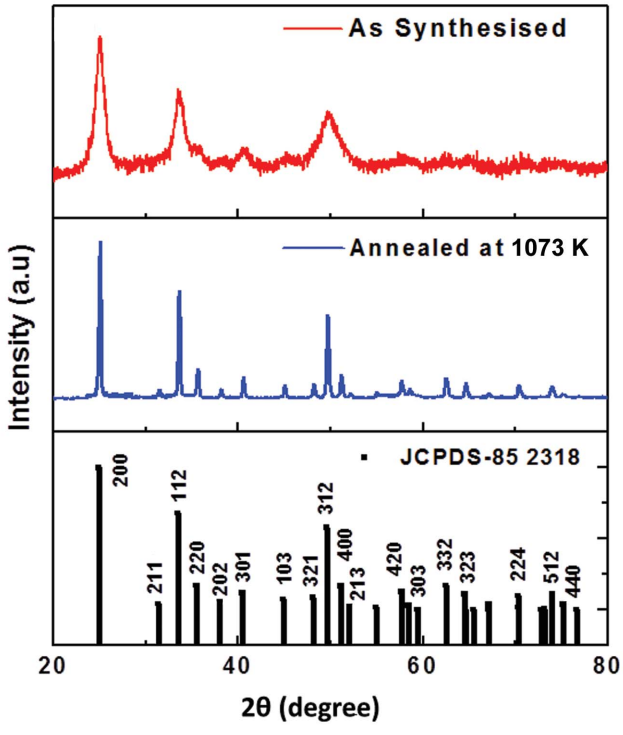

(*a*)

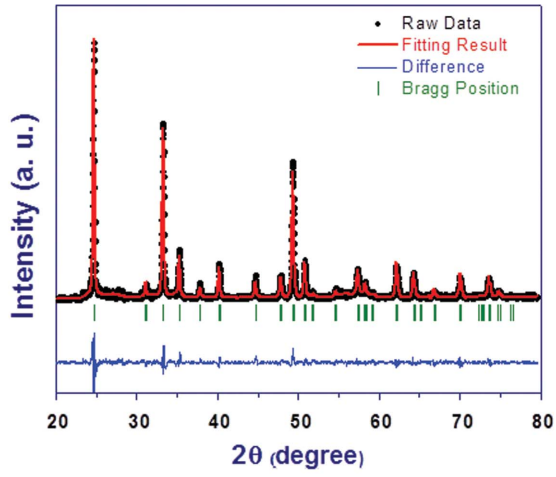

(*b*)

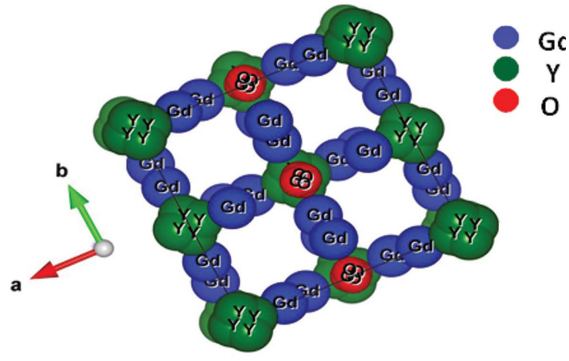

(*c*)

Figure 1
(*a*) XRD pattern of the $Gd_{0.20}Y_{0.77}VO_4$ samples as synthesized by the co-precipitation technique and annealed at 1073 K. (*b*) Rietveld refinement of the XRD data of the $Gd_{0.20}Y_{0.77}VO_4$ sample annealed at 1073 K. The black dots and red line represent the observed and fitted data, respectively. The blue line represents the difference between the observed and fitted data. (*c*) A schematic representation of the structure of $GdYVO_4$.

respectively. The lowering of the band gap of (Gd,Y)VO_4 as compared to YVO_4 is attributed to the fact that the Gd^{3+} ions form some metastable states between the valence band and conduction band (Som *et al.*, 2016).

3.3. Morphological and elemental analysis

The morphology of the $Gd_{0.20}Y_{0.77}VO_4$:Sm^{3+} particles annealed at 1073 K was investigated using scanning electron microscopy (SEM). The sample consists of homogenous aggregates of truncated spherical particles. The energy dispersive X-ray analysis (EDAX) spectrum along with the elemental composition is shown in Fig. 3(*a*).

3.4. Photoluminescence analysis

The photoluminescence (PL) emission spectra of the host lattices YVO_4 and $Gd_{0.20}Y_{0.77}VO_4$ excited at ~311 nm are shown in Fig. 4(*a*). The spectrum shows a broad band PL peaking in the blue (~450 nm) region. The PL excitation and emission spectra of the vanadate samples with optimized Sm^{3+} and Gd^{3+} ion concentrations are shown in Figs. 4(*b*) and 4(*c*).

At 311 nm excitation, three main intensity peaks located at 563, 598 and 644 nm are observed, which are due to the $^4G_{5/2} \rightarrow {}^6H_{5/2}$, $^4G_{5/2} \rightarrow {}^6H_{7/2}$ and $^4G_{5/2} \rightarrow {}^6H_{9/2}$ transitions of Sm^{3+} ions. In the emission spectra, the splitting of emission lines of Sm^{3+} into several lines is due to the crystal field splitting, which shows that Sm^{3+} ions are occupying the low-symmetry sites in the lattice. The emission corresponding to the $^4G_{5/2} \rightarrow {}^6H_{7/2}$ transition has the highest intensity (598 nm) among the emission peaks as it satisfies the selection rule $\Delta J = \pm 1$ (allowed transition). The transition $^4G_{5/2} \rightarrow {}^6H_{5/2}$, which is a magnetic dipole (m.d.) in nature, follows the first condition ($\Delta J = 0$). The next transition $^4G_{5/2} \rightarrow {}^6H_{7/2}$ ($\Delta J = \pm 1$) is again an (m.d.)-allowed one but is dominated by an electric dipole (e.d.) transition. Therefore, it is partly an m.d. and partly an e.d. type transition. The higher intensity of the peak at 598 nm, as compared to that at 648 nm (m.d. transition), signifies the more asymmetric nature of the trivalent Sm^{3+} ions and gives a measure of the degree of distortion from the inversion symmetry of the local environment of the Sm^{3+} ion in the host. Therefore, the high intensity of the e.d. transition (598 nm) as compared to the m.d. transition (648 nm) reveals strong electric fields of low symmetry at the Sm^{3+} ions.

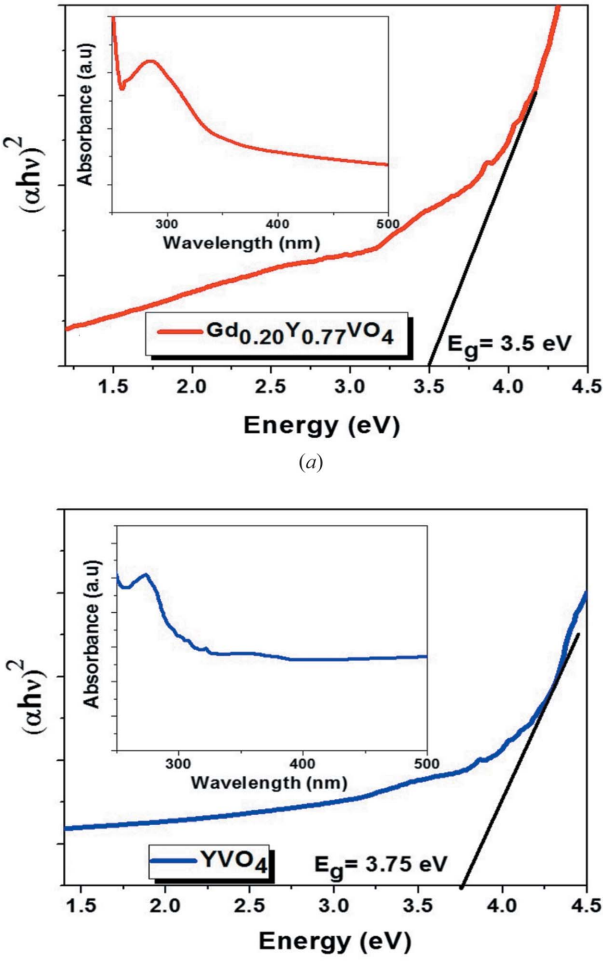

Figure 2
$(\alpha hv)^2$ *versus* energy plot for the determination of the optical band gap of (*a*) $Gd_{0.20}Y_{0.77}VO_4$:Sm^{3+} and (*b*) YVO_4:Sm^{3+} samples. Insets in both figures show their corresponding UV–vis–NIR absorption spectrum.

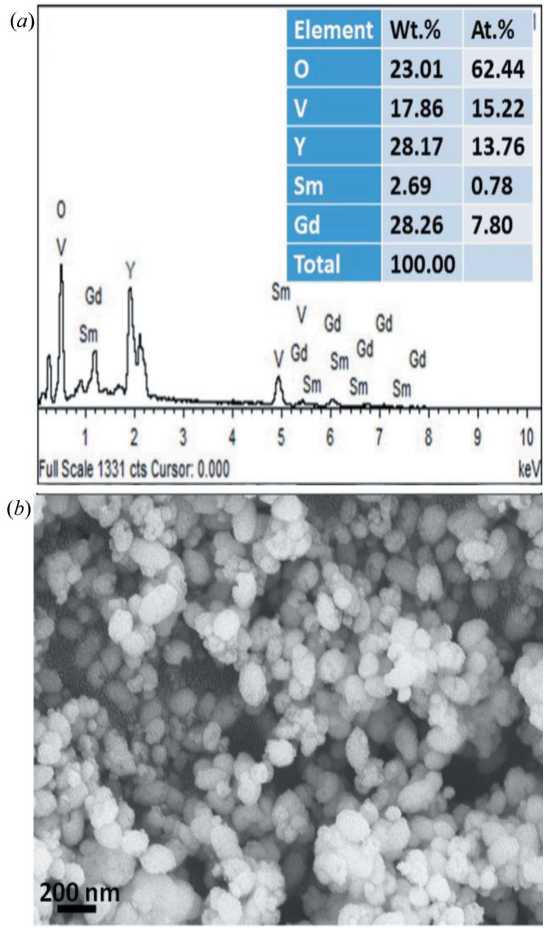

Figure 3
(*a*) A representative EDAX spectrum of a $Gd_xY_{1-x}VO_4$:Sm^{3+}(3%) sample, showing the presence of Sm^{3+} in the material along with the elemental composition. (*b*) SEM micrograph of a $Gd_xY_{1-x}VO_4$:Sm^{3+} nanophosphor annealed at 1073 K.

In the excitation spectra of Fig. 4(*b*), the excitation peak at 311 nm is attributed to the symmetry-allowed $^1A_1 \rightarrow {}^1T_2$ ($t_1 \rightarrow 2e$) absorption of the VO_4^{3-} unit, signifying electron transfer from oxygen 2*p* states to the empty *d* states of the vanadium ion (Liu *et al.*, 2012; Yang *et al.*, 2011; Liu *et al.*, 2006; Ronde & Blasse, 1978; Krumpel *et al.*, 2009). The excitation spectrum reveals that in the case of $Gd_{0.20}Y_{0.77}VO_4$:Sm^{3+} the charge transfer band (CTB) at ~311 nm is quite dominant as compared to the spectrum of YVO_4. This supports the contribution of the Gd^{3+} ion in the charge transfer phenomenon. The optical and corresponding confocal fluorescence images of $Gd_{0.20}Y_{0.77}VO_4$:Sm^{3+}(3%) excited by UV laser (375 nm) light are shown in Figs. 5(*a*) and 5(*b*). Furthermore, the PL spectra shown in Fig. 5(*c*) reveal that the emission intensity of $Gd_{0.20}Y_{0.77}VO_4$:Sm^{3+} is higher than that of YVO_4:Sm^{3+} (for the optimized Sm^{3+} concentration). Actually, in $Gd_xY_{1-x}VO_4$:Sm, the reason behind the enhanced CTB and emission intensity is probably the efficient energy transfer from the VO_4^{3-} network to Sm^{3+} ions mediated by Gd^{3+} ions. Under 311 nm excitation, in the VO_4^{3-} unit the symmetry-allowed $^1A_1 \rightarrow {}^1T_2$ absorption occurs Thereafter, two possibilities may arise, *viz*. either the VO_4^{3-} unit transfers its excitation energy to the activator Sm^{3+} ion or it relaxes to the ground state with the PL emission of blue light. In YVO_4:Sm^{3+} the intensity of blue PL emission is higher than that in $Gd_{0.20}Y_{0.77}VO_4$:Sm^{3+}, while the intensity of orange–red PL emission is lower (see Figs. 4*a* and 5*c*), indicating efficient energy transfer (ET) from VO_4^{3-} to Sm^{3+} in the case of $Gd_{0.20}Y_{0.77}VO_4$. The reason behind the enhanced PL emission intensity in the case of $Gd_xY_{1-x}VO_4$:Sm^{3+} is that the ET from the VO_4^{3-} unit is effectively sensitizing the ^6P_J states of Gd^{3+} ions because of the partial overlap between the VO_4^{3-} emission and $^8S_{7/2}$–^6P_J absorption of Gd^{3+}, and from ^6P_J states the energy is transferred to the Sm^{3+} ions, resulting in an efficient orange–red PL emission (Tian *et al.*, 2008). Apart from this, in the PL emission spectra no peak corresponding to the ^6P_J–$^8S_{7/2}$ transition (*i.e.* ~311 nm) was observed, indicating that Gd^{3+} ions are transferring the excitation energy to the Sm^{3+} ions instead of undergoing ^6P_J–$^8S_{7/2}$ transition (Tian *et al.*, 2008).

Moreover, in the $Gd_{0.20}Y_{0.77}VO_4$ host, the blue PL emission corresponding to the VO_4^{3-} ion transition is significantly reduced as compared to that for YVO_4, indicating that the excitation energy of the VO_4^{3-} units is transferred to Gd^{3+} ions. Actually, the PL emission spectra shown in Fig. 4(*a*) are those of undoped YVO_4 and $Gd_{0.20}Y_{0.77}VO_4$ recorded in the range 400–600 nm without the dopant Sm^{3+} ions. Under UV (311 nm) excitation, the blue emission (which is actually due to the $^3T_1 \rightarrow {}^1A_1$ transition of the VO_4^{3-} ion) is stronger in YVO_4, which signifies that in the case of undoped YVO_4 all the excitation energy absorbed by the VO_4^{3-} ions is released as blue emission due to the $^3T_1 \rightarrow {}^1A_1$ transitions of the VO_4^{3-} ion. When Gd^{3+} ions are introduced into the lattice, the blue emission intensity is reduced because all the excitation energy absorbed by the VO_4^{3-} ions is further transferred to the Gd^{3+} ions, and hence, in the case of undoped $Gd_{0.20}Y_{0.77}VO_4$, all the excitation energy absorbed by the VO_4^{3-} ion is not released as blue emission. Part of this excitation energy is transferred to the Gd^{3+} ions, hence lowering the intensity of the corresponding blue emission. But when Sm^{3+} ions are added into

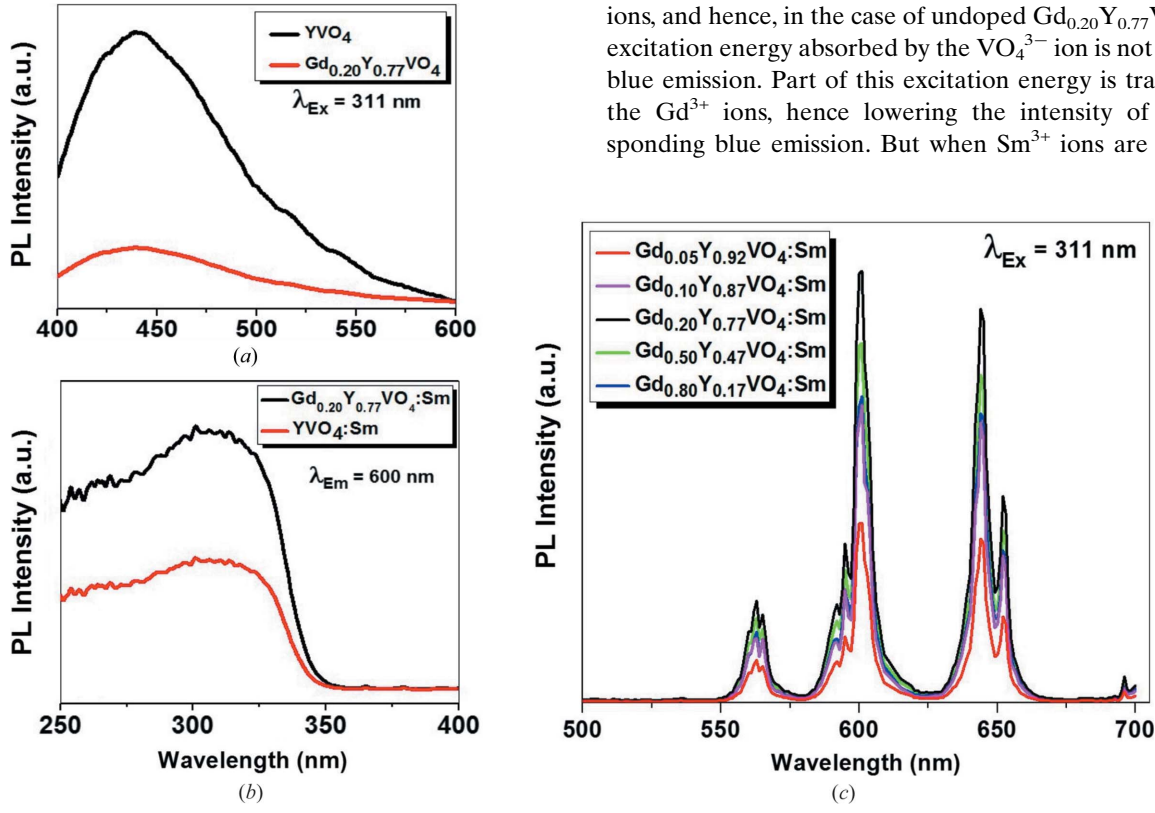

Figure 4
(*a*) The PL emission spectra of YVO_4 and $Gd_{0.20}Y_{0.77}VO_4$ host lattices in the range 400–600 nm under 311 nm excitation. (*b*) PL excitation spectra of $Gd_{0.20}Y_{0.77}VO_4$:Sm^{3+} and YVO_4:Sm^{3+} nanophosphors recorded at 600 nm emission. (*c*) PL emission spectra of $Gd_xY_{1-x}VO_4$:Sm^{3+} (x = 0.05 to 0.80) samples annealed at 1073 K registered at 311 nm excitation with the concentration of Sm fixed at 0.03 moles for all the samples.

the lattice, the Gd^{3+} ions further transfer the excitation energy to the Sm^{3+} ions, resulting in an enhanced orange–red emission in (Gd,Y)VO_4:Sm as compared to YVO_4:Sm samples. This was performed to establish the role of Gd^{3+} ions as intermediates in the energy transfer phenomenon between the VO_4^{3-} ions and Sm^{3+} ions. The results signify that, in (Gd,Y)VO_4:Sm, the excitation energy absorbed by the VO_4^{3-} ions is first transferred to the intermediate Gd^{3+} ions and then finally to the Sm^{3+} ions. Under UV excitation of $Gd_xY_{1-x}VO_4$ compounds, three possible mechanisms affecting luminescence are (i) the sensitization of Gd^{3+} (^6P_J) levels by VO_4^{3-} energy transfer; (ii) migration of excitation energy between Gd^{3+} ions, resulting in enhanced non-radiative transitions; and (iii) the trapping of the excitation energy from Gd^{3+} ions by dopant (Sm^{3+}) ions.

When a small number of Gd^{3+} ions are doped into the lattice, they may occupy the lattice sites, but when the concentration of Gd^{3+} is higher than the optimum, this results in shrinking of the unit cell, which in turn results in migration of excitation energy between Gd^{3+} ions (hopping), thus reducing the corresponding Sm^{3+} ion emission (Juan *et al.*, 2014). Hence, when the concentration of Gd^{3+} ions is higher than the optimum, the excitation energy is not transferred to Sm^{3+} ions; it migrates from one Gd^{3+} ion to another, resulting in reduced emission intensity, as shown in Fig. 6. Moreover, addition of Gd^{3+} into the YVO_4 lattice not only affects the crystal structure but also affects the generated crystal field, which affects the Sm^{3+} emission intensity drastically (Kumari & Manam, 2015). The doping of Gd^{3+} ions in addition slightly changes the volume of the unit cell in the crystal and thereby improves the energy transfer efficiency to Sm^{3+} ions, and eventually increases the fluorescence emission. Thus, the fluorescence emission could be adjusted by Gd^{3+} ion doping. The Gd^{3+} concentration was varied with x = 0, 0.05, 0.10, 0.20, 0.50 and 0.80, *i.e.* from 0 to 80 mol%. The Gd concentration x = 20 mol% generates the most favourable crystal environment for the Sm^{3+} ion and hence the maximum PL emission intensity is observed for the $Gd_{0.20}Y_{0.77}VO_4$:Sm^{3+}(3%) phosphor under UV excitation (Kumari & Manam, 2015).

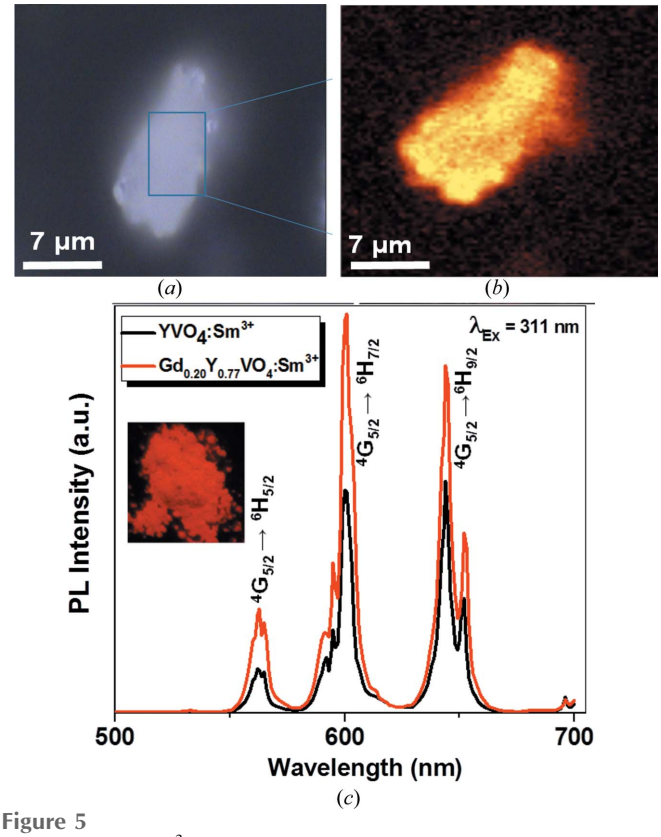

Figure 5
$Gd_{0.20}Y_{0.77}VO_4$:Sm^{3+}(3%): (*a*) optical image and (*b*) confocal fluorescence image under UV laser (375 nm) light excitation. (*c*) PL emission spectra of Sm^{3+} doped YVO_4 and $Gd_{0.20}Y_{0.77}VO_4$ samples under 311 nm excitation. The inset shows an image of orange–red emitting $Gd_{0.20}Y_{0.77}VO_4$:Sm^{3+} (3%) nanophosphor under UV (370 nm) light.

3.5. Time-resolved photoluminescence decay analysis

The intermediate role of Gd^{3+} ions in energy transfer has in addition been established using time-resolved PL, also known as lifetime decay measurements. Fig. 7 shows the decay curves of Sm^{3+} doped $Gd_{0.20}Y_{0.77}VO_4$ and YVO_4 samples under 311 nm excitation. Luminescence decay measurements are used for establishing energy transfer mechanisms and

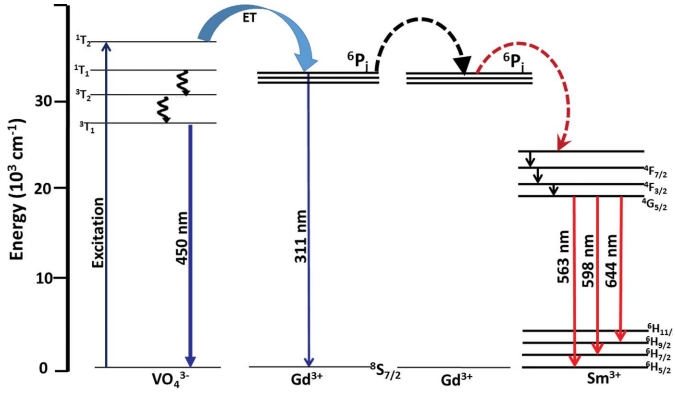

Figure 6
Energy level diagram showing the energy transfer mechanism in $Gd_xY_{1-x}VO_4$:Sm^{3+} samples with Gd^{3+} ions as intermediates.

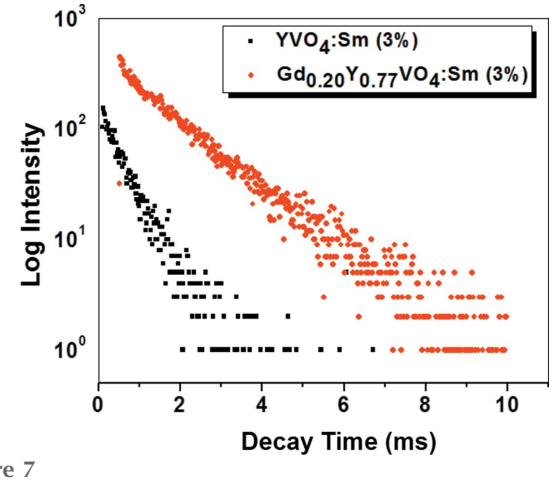

Figure 7
Time-resolved photoluminescence decay curve of Sm^{3+} doped YVO_4 and $Gd_{0.20}Y_{0.77}VO_4$ nanophosphor samples.

Table 2
Decay parameters of Sm^{3+} doped YVO_4 and $Gd_{0.20}Y_{0.77}VO_4$ nanophosphor samples generated from the curve fitting.

Sample code	τ_1 (ms)	τ_2 (ms)
$YVO_4:Sm^{3+}$(3%)	0.025	0.44
$Gd_{0.20}Y_{0.77}VO_4:Sm^{3+}$(3%)	0.025	0.529

luminescence quenching phenomena. The double exponential decay behaviour of the activator is often observed when the excitation energy is transferred from the donor (Shen *et al.*, 2005). The resulting time-resolved PL decay curves were fitted *via* a multiexponential equation:

$$I(t) = I_0 + A_1 \exp(-t/\tau_1) + A_2 \exp(-t/\tau_2), \qquad (8)$$

where τ_1 and τ_2 are the fast and slow components of the luminescent lifetimes, and A_1 and A_2 are the respective fitting parameters. The decay parameters are listed in Table 2. The decay rate of $Gd_{0.20}Y_{0.77}VO_4:Sm^{3+}$ is slower than that of $YVO_4:Sm^{3+}$, indicating that with the addition of Gd^{3+} ions an extra pathway is introduced in the energy transfer phenomenon, thereby enhancing the decay rate. Firstly, energy is transferred from VO_4^{3-} to Gd^{3+}; afterwards, this excitation energy is trapped by the dopant Sm^{3+} ions, which increases the VO_4^{3-} overall decay rate. This further supports the role of Gd^{3+} ions as intermediates for efficient energy transfer from VO_4^{3-} to Sm^{3+} (Wei *et al.*, 2011)

3.6. CIE colour coordinates

The corresponding CIE (Commission Intemationale de I'Eclairage 1931 chromaticity) coordinate positions of $Gd_{0.20}Y_{0.77}VO_4:Sm^{3+}$ were calculated and are presented in Fig. 8. The CIE chromaticity coordinates were determined using PL data recorded at an interval of 1 nm which were fed into an in-house developed program based on the equidistant wavelength method (Kelmer, 1969). The corresponding values are (x = 0.59, y = 0.38), which lies in the orange–red region, specifically where the spectral response of Si solar cells is significantly high.

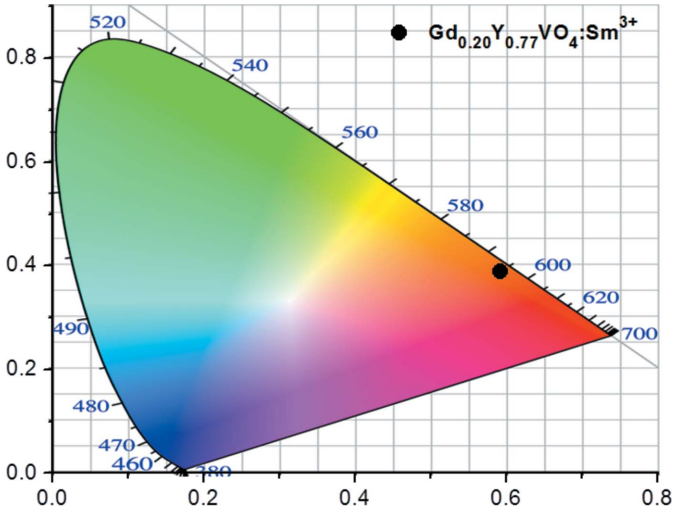

Figure 8
CIE diagram of the Sm^{3+} doped $Gd_{0.20}Y_{0.77}VO_4$ nanophosphor showing the colorimetric coordinates.

4. Conclusion

In this work, Sm^{3+} doped $Gd_xY_{1-x}VO_4$ phosphors with different Gd concentrations (0–80 mol%) have been successfully synthesized by the chemical co-precipitation method. The XRD pattern and Rietveld analysis confirmed that the synthesized phosphor crystallizes in a single phase with a tetragonal structure. The role of Gd^{3+} ions as intermediates in emission enhancement has been successfully established with UV, PL and time-resolved PL decay measurements. The optical band gaps of YVO_4 and $Gd_{0.20}Y_{0.77}VO_4$ have been approximated from the UV–vis–NIR absorption spectra to be 3.75 and 3.50 eV, respectively. Under 311 nm excitation, the emission intensity of $Gd_{0.20}Y_{0.77}VO_4:Sm^{3+}$ phosphor is the highest, with the optimum Gd^{3+} (20 mol%) and Sm^{3+} (3 mol%) concentration. The PL emission intensity of $Gd_{0.20}Y_{0.77}VO_4:Sm^{3+}$ is enhanced as compared to that of $YVO_4:Sm^{3+}$, for the optimized Sm^{3+} concentration. The combination of their unique features of high surface-to-volume ratios, monodispersion and optimum photoluminescence suggests that these nanophosphors will find many interesting applications in semiconductor photophysics, inorganic light-emitting diodes, solar cells and nanodevices.

Funding information

Funding for this research was provided by: Council of Scientific and Industrial Research (CSIR) (award Nos. 31/1(445)/2015-EMR-1, 31/1(448)/2015-EMR-1); Board of Research in Nuclear Sciences (BRNS) (award No. 34/14/16/2016-BRNS/34041).

References

Braga, A. F. B., Moreira, S. P., Zampieri, P. R., Bacchin, J. M. G. & Mei, P. R. (2008). *Solar Energy Mater. Solar Cells*, **92**, 418–424.
Chen, H. M., Chen, C. K., Liu, R. S., Zhang, L., Zhang, J. & Wilkinson, D. P. (2012). *Chem. Soc. Rev.* **41**, 5654–5671.
Chen, L., Chen, K. J., Hu, S. F. & Liu, R. S. (2011). *J. Mater. Chem.* **21**, 3677–3685.
Chen, X., Li, C., Grätzel, M., Kostecki, R. & Mao, S. S. (2012). *Chem. Soc. Rev.* **41**, 7909–7937.
Heng, C. L., Wang, T., Su, W. Y., Wu, H. C., Yin, P. G. & Finstad, T. G. (2016). *J. Appl. Phys.* **119**, 123105–123107.
Hisatomi, T., Kubota, J. & Domen, K. (2014). *Chem. Soc. Rev.* **43**, 7520–7535.
Juan, Y., Jian-Bei, Q., Yu-An, W. & Da-Cheng, Z. (2014). *Chin. Phys. B*, **23**, 104224–104227.
Kelmer, J. (1969). *Luminescent Screens: Photometry and Colorimetry*, p. 118. London: Iliffe.
Krumpel, A. H., van der Kolk, E., Cavalli, E., Boutinaud, P., Bettinelli, M. & Dorenbos, P. (2009). *J. Phys. Condens. Matter*, **21**, 115503–115508.

Kumari, P. & Manam, J. (2015). *RSC Adv.* **5**, 107575–107584.
Liu, D., Shi, J., Tong, L., Ren, X., Li, Q. & Yang, H. (2012). *J. Nanopart. Res.* **14**, 1216–1223.
Liu, G., Hong, G., Wang, J. & Dong, X. (2006). *Nanotechnology*, **17**, 3134–3138.
Pinel, P., Cruickshank, C. A., Beausoleil-Morrison, I. & Wills, A. (2011). *Renewable Sustainable Energy Rev.* **15**, 3341–3359.
Ronde, H. & Blasse, G. J. (1978). *J. Inorg. Nucl. Chem.* **40**, 215–219.
Shen, W. Y., Pang, M. L., Lin, J. & Fang, J. (2005). *J. Electrochem. Soc.* **152**, H25–H28.
Som, S., Kumar, V., Kumar, V., Gohain, M., Pandey, A., Duvenhage, M. M., Terblans, J. J., Bezuindenhoud, B. C. B. & Swart, H. C. (2016). *Ultrason. Sonochem.* **28**, 79–89.
Tian, Z., Liang, H., Han, B., Su, Q., Tao, Y., Zhang, G. & Fu, Y. (2008). *J. Phys. Chem. C*, **112**, 12524–12529.
Wang, J., Xu, Y., Hojamberdiev, M., Cui, Y., Liu, H. & Zhu, G. (2009). *J. Alloys Compd.* **479**, 772–776.
Wegh, R. T., Donker, H., Oskam, K. D. & Meijerink, A. (1999). *J. Lumin.* **82**, 93–104.
Wei, X., Liu, Y., Jiang, G., Chen, Y., Yin, M. & Xu, W. (2011). *J. Nanosci. Nanotechnol.* **11**, 9556–9561.
Yang, H. K., Moon, B. K., Choi, B. C., Jeong, J. H. & Kim, K. H. (2011). *CrystEngComm*, **13**, 4723–4728.
Zhydachevskii, Y., Lipińska, L., Baran, M., Berkowski, M., Suchocki, A. & Reszka, A. (2014). *Mater. Chem. Phys.* **143**, 622–628.
Zou, Z., Ye, J., Sayama, K. & Arakawa, H. (2001). *Nature*, **414**, 625–627.